MIT Libraries | DSpace@MIT

MIT Open Access Articles

SUPERNOVA REMNANT KES 17: AN EFFICIENT COSMIC RAY ACCELERATOR INSIDE A MOLECULAR CLOUD

The MIT Faculty has made this article openly available. ***Please share*** how this access benefits you. Your story matters.

Citation: Gelfand, Joseph D., Daniel Castro, Patrick O. Slane, Tea Temim, John P. Hughes, and Cara Rakowski. "SUPERNOVA REMNANT KES 17: AN EFFICIENT COSMIC RAY ACCELERATOR INSIDE A MOLECULAR CLOUD." The Astrophysical Journal 777, no. 2 (October 23, 2013): 148. © 2013 American Astronomical Society.

As Published: http://dx.doi.org/10.1088/0004-637x/777/2/148

Publisher: Institute of Physics/American Astronomical Society

Persistent URL: http://hdl.handle.net/1721.1/93916

Version: Final published version: final published article, as it appeared in a journal, conference proceedings, or other formally published context

Terms of Use: Article is made available in accordance with the publisher's policy and may be subject to US copyright law. Please refer to the publisher's site for terms of use.

Massachusetts Institute of Technology

The Astrophysical Journal, 777:148 (12pp), 2013 November 10 doi:10.1088/0004-637X/777/2/148
© 2013. The American Astronomical Society. All rights reserved. Printed in the U.S.A.

SUPERNOVA REMNANT KES 17: AN EFFICIENT COSMIC RAY ACCELERATOR INSIDE A MOLECULAR CLOUD

Joseph D. Gelfand[1,7], Daniel Castro[2], Patrick O. Slane[3], Tea Temim[4,8], John P. Hughes[5], and Cara Rakowski[6]
[1] NYU Abu Dhabi, P.O. Box 903, New York, NY 10276, USA; jg168@cosmo.nyu.edu
[2] MIT Kavli Institute for Astrophysics & Space Research, 77 Massachusetts Avenue 37-241, Cambridge, MA 02139, USA
[3] Harvard-Smithsonian Center for Astrophysics, 60 Garden Street, Cambridge, MA 02138, USA
[4] Observational Cosmology Lab, Code 665, NASA Goddard Space Flight Center, Greenbelt, MD 20771, USA
[5] Department of Physics and Astronomy Rutgers University 136 Frelinghuysen Road, Piscataway, NJ 08854, USA
[6] United States Patent and Trademark Office, 600 Dulany Street, Alexandria, VA, USA; cara.rakowski@gmail.com
Received 2012 November 3; accepted 2013 September 17; published 2013 October 23

ABSTRACT

The supernova remnant Kes 17 (SNR G304.6+0.1) is one of a few but growing number of remnants detected across the electromagnetic spectrum. In this paper, we analyze recent radio, X-ray, and γ-ray observations of this object, determining that efficient cosmic ray acceleration is required to explain its broadband non-thermal spectrum. These observations also suggest that Kes 17 is expanding inside a molecular cloud, though our determination of its age depends on whether thermal conduction or clump evaporation is primarily responsible for its center-filled thermal X-ray morphology. Evidence for efficient cosmic ray acceleration in Kes 17 supports recent theoretical work concluding that the strong magnetic field, turbulence, and clumpy nature of molecular clouds enhance cosmic ray production in supernova remnants. While additional observations are needed to confirm this interpretation, further study of Kes 17 is important for understanding how cosmic rays are accelerated in supernova remnants.

Key words: cosmic rays – gamma rays: ISM – ISM: individual objects (Kes 17) – ISM: supernova remnants – X-rays: individual (Kes 17)

Online-only material: color figures

1. INTRODUCTION

Supernova remnants (SNRs) are believed to be important in both forming and regulating the multi-phase interstellar medium (ISM) found inside star-forming galaxies (e.g., McKee & Ostriker 1977), distributing metals produced in the progenitor explosion throughout the host galaxy, producing dust (e.g., Salpeter 1977), and accelerating cosmic rays up to energies $E \sim 10^{15.5}$ eV (e.g., Arnett & Schramm 1973). However, direct observational evidence supporting this last assertion is rare. While several Milky Way SNRs are identified as cosmic ray producers, only one (Tycho's SNR) shows evidence for accelerating protons up to the "knee" in the cosmic ray spectrum believed to delineate Galactic from extragalactic cosmic rays (Eriksen et al. 2011).

Determining whether SNRs are responsible for the observed cosmic ray population requires studying individual remnants to determine both if and how they accelerate cosmic rays. SNRs are extremely complicated objects comprised of hot ISM material shocked by the expanding supernova blast wave (the "forward shock"), supernova ejecta heated by the shock wave driven into the SNR by the shocked ISM (the "reverse shock"), cold unshocked ejecta, and relativistic electrons and ions accelerated at the forward and/or reverse shock. Additionally, the dynamical evolution of the SNR strongly depends on its surroundings (e.g., Lozinskaya 1992). Determining the properties of relativistic particles accelerated inside an SNR first requires measuring the physical properties of these different components.

This requires analyzing an SNR's emission across the entire electromagnetic spectrum. An SNR's radio emission traces GeV electrons accelerated in the remnant. Its infrared (IR) emission is produced by dust and atomic and molecular gas inside and outside the SNR heated by shocks and higher energy emission. A remnant's thermal X-ray emission traces both ISM material shocked by the forward shock and ejecta shocked by the reverse shock. Finally, its γ-ray emission traces relativistic electrons, and possibly hadrons (cosmic rays), accelerated in the SNR (e.g., Ackermann et al. 2013). Due to new observing capabilities at both IR wavelengths (e.g., *Spitzer*, *AKARI*, and *Herschel*) and γ-ray energies (e.g., *Fermi*, H.E.S.S, V.E.R.I.T.A.S, and MAGIC), the number of SNRs detected in all four wavebands is rapidly increasing. One such remnant is Kes 17 (SNR G304.6+0.1). In this paper, we analyze recent radio, IR, X-ray, and γ-ray observations of this remnant (Section 2) and use these results to determine the physical properties of this SNR and its surroundings (Section 3). Finally, we summarize our results and discuss their implications on the interaction between SNRs and their environments (Section 4).

2. OBSERVATIONS AND DATA ANALYSIS

In this section, we analyze recent radio (Section 2.1), IR (Section 2.2), X-ray (Section 2.3), and γ-ray (Section 2.4) observations of this source.

2.1. Radio

Kes 17 was first detected at 408 MHz and 5 GHz by Shaver & Goss (1970) who, based on the non-thermal spectrum implied by its flux at these two frequencies, classified this source as an SNR. This identification was supported by the detection of polarized 5 GHz emission (Milne & Dickel 1975) and the irregular shell-like morphology revealed by analysis of data taken during the Molonglo Observatory Synthesis Telescope (MOST) Galactic plane survey (Whiteoak & Green 1996). Analysis of the H I spectrum using the standard H I absorption method toward Kes 17 suggests a distance $d > 9.7$ kpc (Caswell et al. 1975).

[7] Affiliate Member, Center for Cosmology and Particle Physics, New York University.
[8] Oak Ridge Associated Universities, Oak Ridge, TN 37831, USA.

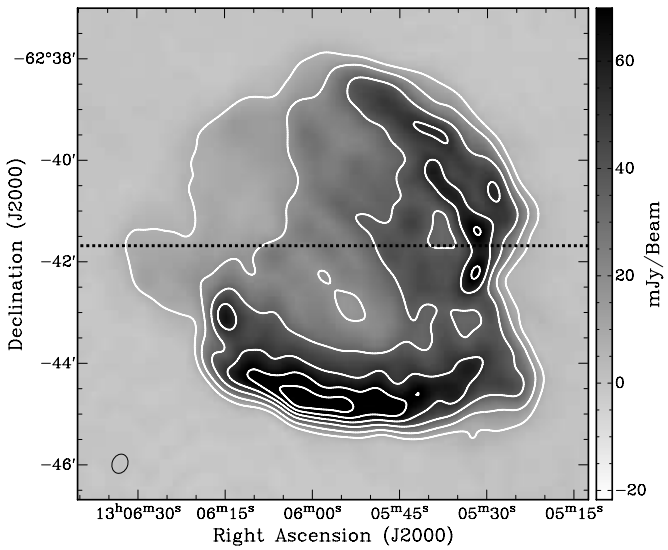

Figure 1. 1.4 GHz image of Kes 17. The total intensity image was made from the combined data described in Section 2.1 using uniform weighting, multi-frequency synthesis, and maximum entropy deconvolution. This image has an rms noise of 0.72 mJy beam^{-1} and a resolution of 23.″3 × 18.″4 (size and orientation of beam represented by the ellipse in the lower left-hand corner.) The white contours indicate surface brightness levels of 10σ, 25σ, 50σ, 75σ, and 100σ. The dashed line indicates the region used to make the brightness profile shown in Figure 2.

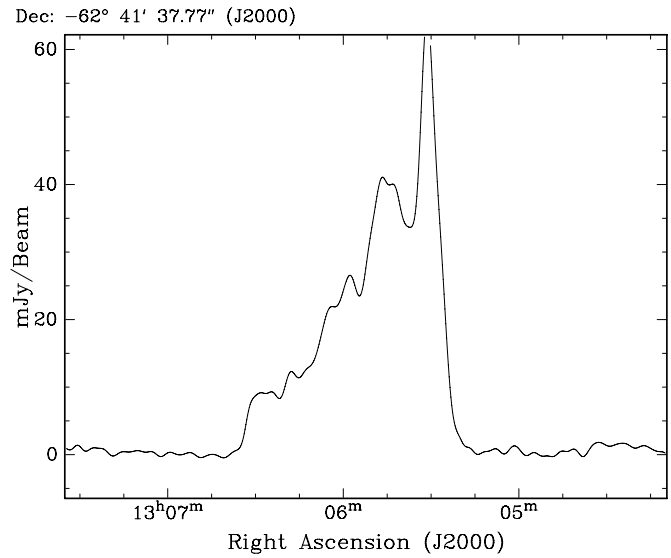

Figure 2. 1.4 GHz intensity profile of Kes 17 along a line of constant declination $\delta = -62°41'37.''77$ (J2000). At this declination, Kes 17 has the largest angular extent.

Table 1
Flux Densities of Kes 17 at Several Radio Frequencies

Frequency (GHz)	Flux Density (Jy)	Reference
0.408	29.8	Shaver & Goss (1970)
0.843	18	Whiteoak & Green (1996)
1.4	10.9 ± 0.14	This work
5.0	6.7	Shaver & Goss (1970)

Last, but not least, the detection of OH (1720 MHz) maser emission (Frail et al. 1996) requires the presence of shocked molecular material (Elitzur 1976; see Wardle & McDonnell 2012 for a recent review).

The Australia Telescope Compact Array, while in its 1.5A configuration, observed this SNR on 2004 March 14 at both 1.4 & 2.4 GHz. This observation used the correlator setting with the maximum bandwidth available (128 MHz bands over 13 channels), with one band centered at 1384 MHz and the other at 2368 MHz. This observation recorded all four linear polarization modes (XX, YY, XY, and YX). We used the MIRIAD software package (Sault et al. 1995) to calibrate the flux density using an observation of PKS B1934-638, calibrate the phase using data from regular observations of PKS 1329−665, and image the Kes 17 data. To improve our sensitivity to diffuse 1.4 GHz emission in the field, we combined the 1.4 GHz visibilities of Kes 17 with continuum data from the Southern Galactic Plane Survey (McClure-Griffiths et al. 2005).

As shown in Figure 1, at 1.4 GHz this SNR has a partial shell morphology with a diameter of ∼7.′5 dominated by two rims in the S and NW regions connected by a "notch"-like feature in the SW. While the NE region has a surface brightness about six times lower than the S and NW rims, there is a sharp decrease in flux density that defines the edge of this remnant (Figure 2). Diffuse radio emission is also detected interior to the shell (Figures 1 and 2). The total (Stokes I) 1.4 GHz flux density of Kes 17 is 10.9±0.14 Jy and no polarized emission was detected (Table 1). The lack of data with short u–v spacing at 2.4 GHz precluded making a similar quality image and flux density measurement at this higher frequency.

2.2. Infrared

The first IR detection of Kes 17 was made with the *Infrared Astronomical Satellite* (*IRAS*), which revealed shell-like emission from this SNR (Arendt 1989). More recent *Spitzer* Infrared Array Camera (IRAC) observations from the GLIMPSE survey uncovered very bright emission in the 3.6–8.0 μm bands (Lee 2005; Reach et al. 2006) from a more diffuse SNR shell. The filamentary structure along the NW rim is particularly bright at 4.5 μm, suggesting that the emission originates from shocked H_2. Based on the colors and morphological similarities of the IRAC images, Reach et al. (2006) concluded that this emission is produced by molecular shocks.

Analysis of 5–38 μm spectroscopic follow-up observations by the Infrared Spectrograph (IRS) on board *Spitzer* revealed bright pure rotational lines of H_2, most likely indicating an interaction between the SNR and dense molecular material (Hewitt et al. 2009). Shock models suggest that the excitation of the observed H_2 lines requires two shock components: a slower 10 km s^{-1} C-shock through denser clumps with $n_0 = 10^6$ cm^{-3}, and a faster 40 km s^{-1} C-shock passing through a lower density medium with $n_0 = 10^4$ cm^{-3} (Hewitt et al. 2009). Analyses of the spectra also reveal atomic fine-structure lines of Fe II, Ne II, Ne III, S III, S I, and S II, whose relative emission line fluxes lead to densities in the 100–1000 cm^{-3} range and shock velocities of 150–200 km s^{-1} (Hewitt et al. 2009).

Most recently, the broadband mid-to far-IR emission from Kes 17 was detected by the Multiband Imaging Photometer for Spitzer (MIPS) at 24 μm (Lee et al. 2011; Pinheiro Gonçalves et al. 2011) and the *AKARI* satellite at 15, 24, 65, 90, 140, and 160 μm (Lee et al. 2011). Emission at these wavelengths is concentrated in the W and S shells, partially overlapping with the W radio rim. The broadband IR spectral energy distribution is well fit by two modified blackbodies with a mixture of carbonaceous and silicate dust grain compositions. The best fit temperatures are 79 ± 6 K and 27 ± 3 K with dust masses of 6.2×10^{-4} $M_\odot$ for the hot component and 6.7 $M_\odot$ for the cold

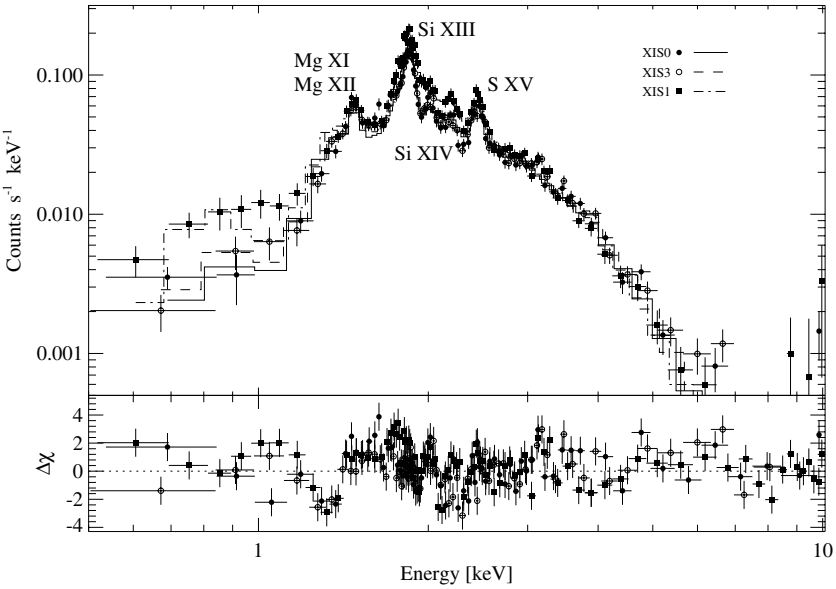

Figure 3. *Suzaku* X-ray spectrum of Kes 17, overlaid with the prediction of the `phabs` × `vnei` model given in Table 2.

component for a distance of 8 kpc (Lee et al. 2011). While this distance is modestly inconsistent with that estimated from the H I absorption spectrum of this SNR (Section 2.1), this discrepancy does not significantly change these masses.

2.3. X-Ray

X-ray emission from Kes 17 was first detected in an unpublished ∼11 ks *ASCA* observation (ObsID 57013000) on 1999 February 12. *XMM-Newton* then observed this SNR on 2005 August 12 (ObsID 0303100201) for ∼20 ks after the removal of background flares (Combi et al. 2010). Analysis of this observation revealed the X-ray emission was diffuse and extended, brightest inside the radio shell, and suggested the presence of both non-thermal and thermal X-ray emission components and spatial variations in its X-ray spectrum (Combi et al. 2010).

More recently, Kes 17 was observed on 2010 September 3 by the *Suzaku* observatory for ∼100 ks (ObsID 505074010). We first reprocessed the *Suzaku* data using the new aepipeline task in the `ftools v6.11` software package[9] (Blackburn 1995), then used a circular region 4′.7 in radius centered on Kes 17 to extract its spectrum, determining the background spectrum using data from an annulus between 4′.7 and 7′.4 in radius also centered on Kes 17. For consistency, we used the same source and background region for all three detectors. The spectra were created using `xselect`, as were the RMF and ARF of the source spectrum. We then fit the observed, background subtracted 0.5–10 keV spectrum to different emission models using the `Sherpa` (Freeman et al. 2001) software package, checking our results with `XSpec` (Arnaud 1996) since these packages use different algorithms to determine the best fit and errors on the model parameters.

Due to the arcminute angular resolution of *Suzaku*, our spectra are contaminated by unrelated objects in the source region. Our analysis of the previous *XMM* observation indicates three bright soft X-ray sources, most likely foreground stars, located within the *Suzaku* source region—one ∼30 times brighter than the other two combined. Our spectral analysis of their combined emission finds it is well reproduced by a Raymond–Smith plasma with $N_{\rm H} \equiv 0$ and solar (Anders & Grevesse 1989) abundances. Since emission from these sources are in the *Suzaku* spectra, we included such a component in all the spectral fits described below, with the temperature and normalization as free parameters. For each fit, the properties of this component are consistent with that measured for the brightest star in the *XMM* data—confirming the foreground origin of this emission.

As shown in Figure 3, there are several prominent lines in the X-ray spectrum of Kes 17, most notably Mg XI and possibly Mg XII at ∼1.5 keV, Si XIII and Si XIV at ∼2 keV, and S XV at ∼2.5 keV, indicative of thermal emission. For most thermal models, assuming the emitting plasma has solar abundances results in fits that underpredict the flux of these Mg lines and overpredict the flux of these S lines. To investigate if these discrepancies result from uncertain calibration of the XIS1 detector around the Si K line, we re-fit the data excluding these channels assuming solar abundances. However, the same feature was observed in the residuals of XIS0 and XIS3 data. Therefore, we allowed the abundance of both Mg and S to vary in our fits.

As shown in Table 2, modeling the thermal X-ray emission with a non-equilibrium ionization model (e.g., the `vnei` model in `XSpec` and `Sherpa`) results in an excellent fit (reduced $\chi^2 \approx 0.8$) for an electron temperature of $kT_{\rm e} \sim 0.7$ keV, sub-solar abundance of S but a super-solar abundance of Mg, and a very large ionization timescale τ ($\tau \gtrsim 2 \times 10^{12}$ cm^{-3} s with 90% confidence), close to the equilibrium ionization condition (Smith & Hughes 2010). A large τ was also reported by Gok & Sezer (2012) in their independent analysis of this *Suzaku* observation. Not surprisingly, modeling the observed spectrum with the Raymond & Smith (1977) model for a diffuse hot plasma, which assumes ionization equilibrium, also provides a very good fit to the data for a similar electron temperature and abundances (Table 2). However, these models assume that the plasma has a constant uniform temperature and a single ionization state (i.e., all the plasma was shocked at the same time to the same temperature), which is unlikely to be true for an SNR. As a result, we also fit the observed X-ray spectrum of Kes 17 with more physically motivated models that allow for a range of temperatures but a single ionization state (`vgnei` and `vsedov`) or a single temperature but a range

[9] Available at http://heasarc.gsfc.nasa.gov/ftools/.

Table 2
Results from Jointly Fitting the X-Ray Spectrum of Kes 17 Measured by All Three Detectors of *Suzaku*

Parameters	`vnei`	`vray`	`vgnei`	`vsedov`	`vpshock`	`vnpshock`
$N_{\rm H}$ (10^{22} cm^{-2})	$3.79^{+0.07}_{-0.14}$	$3.69^{+0.13}_{-0.13}$	$3.72^{+0.09}_{-0.09}$	$3.97^{+0.73}_{-0.15}$	$3.78^{+0.05}_{-0.05}$	$4.22^{+0.04}_{-0.10}$
kT_e (keV)	$0.76^{+-0.03}_{-0.01}$	$0.76^{+0.02}_{-0.02}$	$0.76^{+0.03}_{-0.03}$	$0.54^{+0.03}$	$0.76^{+0.03}_{-0.01}$	$1.37^{+0.17}_{-0.03}$
$kT_{\rm shock}$ (keV)	...	...	...	$0.58^{+0.16}$	...	$0.51^{+1.15}_{-0.07}$
$\langle kT \rangle$ (keV)	...	...	$1.1^{+0.26}_{-0.12}$	...	...	...
[Mg]	$1.69^{+0.23}_{-0.29}$	$1.71^{+0.31}_{-0.28}$	$\equiv 1$	$\equiv 1.7$	$1.68^{+0.23}_{-0.21}$	$\equiv 1$
[S]	$0.58^{+0.07}_{-0.07}$	$0.62^{+0.07}_{-0.07}$	$0.58^{+0.07}_{-0.07}$	$0.68^{+0.28}_{-0.37}$	$0.56^{+0.08}_{-0.06}$	$0.69^{+0.15}_{-0.08}$
τ (cm^{-3} s)	$>2 \times 10^{12}$	...	$2.7^{+0.4}_{-0.3} \times 10^{11}$	$7.7_{-1.8} \times 10^{11}$	5×10^{13}	$6.3^{+23}_{-0.6} \times 10^{10}$
K	$0.038^{+0.002}_{-0.003}$	$0.032^{+0.003}_{-0.002}$	$0.036^{+0.003}_{-0.003}$	$0.050^{+0.009}_{-0.012}$	$0.038^{+0.002}_{-0.004}$	$0.071^{+0.001}_{-0.005}$
Foreground Source						
kT (keV)	$0.65^{+0.13}_{-0.15}$	$0.66^{+0.12}_{-0.15}$	$0.66^{+0.12}_{-0.14}$	$0.67^{+14}_{-0.66}$	$0.65^{+0.14}_{-0.16}$	$0.83_{-0.12}$
K ($\times 10^{-5}$)	$1.11^{+0.41}_{-0.29}$	$1.12^{+0.29}_{-0.29}$	$1.13^{+0.29}_{-0.29}$	$1.13^{+1.43}_{-0.50}$	$1.06^{+0.40}_{-0.22}$	$1.81^{+0.60}_{-0.62}$
χ^2	1290.86	1242.07	1273.04	1813.52	1291.76	1848.89
dof	1628	1629	1628	1628	1628	1628

Notes. The first row indicates the model used to fit the emission from SNR Kes 17, and in each case it was multiplied by the `phabs` model to account for photoelectric absorption. For all fits, the foreground emission mentioned in Section 2.3 is modeled using a $N_{\rm H} \equiv 0$ Raymond–Smith plasma with solar abundances. τ indicates the ionization timescale (defined in Section 3.2), and K the normalization (defined in Section 3.2; Arnaud 1996). For the `vgnei` model, $\langle kT \rangle$ is ionization timescale averaged plasma temperature. For the `vpshock` and `vnpshock` models, τ is the highest ionization timescale in the plasma—the lowest value was fixed at $\tau_l \equiv 0$. The abundance of Mg in the `vgnei` model was fixed to solar since this was the preferred value when it was allowed to vary. For the `vnpshock` and `vsedov` models, the fits preferred unphysical Mg abundances, so it was fixed to the quoted values. Where given, errors denote the 90% confidence region; otherwise, the model was not able to constrain the value of this parameter. Lastly, "dof" stands for degrees of freedom.

of ionization timescales (`vpshock` and `vnpshock`). Of these more physically motivated models, only `vgnei` was able to reproduce the observed spectrum (Table 2). This model does not require a super-solar abundance of Mg, and prefers an ionization timescale $\tau \sim 3 \times 10^{11}$ cm^{-3} s, significantly lower than that required by the other models (Table 2).

The success of purely thermal models in reproducing the observed X-ray spectrum stands in contrast to the past analyses of Gok & Sezer (2012) and Combi et al. (2010) which require substantial non-thermal emission. In their analysis of the same *Suzaku* data, Gok & Sezer (2012) reproduce the electron temperature and Mg and S abundances given in Table 2, but they require a power-law component with photon index $\Gamma \sim 1.4$. (They use a thermal model which assumes ionization equilibrium, consistent with the Raymond–Smith model described above.) The power-law component is motivated by an excess of emission below 1.5 keV resulting from fitting the observed spectrum with a single thermal model (Figure 3 in Gok & Sezer 2012). In our spectral fits, this energy range is dominated by the foreground component described above. The similarity between the properties of our foreground component and the X-ray spectral properties of these stars measured by our analysis of the *XMM* observation establishes a strong case for a purely thermal description of the *Suzaku* X-ray emission from Kes 17.

However, this does not explain the non-thermal X-ray emission claimed by Combi et al. (2010) in their analysis of the *XMM* data. These authors divided Kes 17 into three spatial regions (none of which included the foreground stars mentioned above) and required a significant power-law component with $\Gamma \sim 1$–3 to reproduce the observed emission >4 keV (Figure 2 in Combi et al. 2010) in each region. Our analysis of the *XMM* data following their procedure confirms this result. Even if one does not divide the observed X-ray emission of Kes 17 into three spatial regions, a non-thermal component is still needed to explain the X-ray spectrum measured by *XMM*—fitting the composite X-ray spectrum of Kes 17 as measured with *XMM* with a single absorbed Raymond–Smith plasma with non-solar Mg and S abundances[10] systematically underpredicts the flux >4 keV. Adding a power-law component to this model improves the fit, reducing the χ^2 to 1665.22 with 1605 degrees of freedom. This power-law component has a normalization $K_{\rm PL} = 2.0^{+6.3}_{-1.9} \times 10^{-2}$ photons cm^{-2} s^{-1} keV^{-1} at 1 keV (errors denote the 90% confidence interval) and a photon index $\Gamma = 7.5^{+2.3}_{-3.6}$. These are marginally consistent with the analysis of Combi et al. (2010), who report a total $K_{\rm PL} \sim 10^{-3}$ photons cm^{-2} s^{-1} keV^{-1} at 1 keV a photon index $\Gamma = 3.1 \pm 0.3$ in the northern region which they claim dominates the non-thermal X-rays emission. This photon index is significantly softer than the non-thermal X-ray emission detected from other SNRs (e.g., Reynolds 2008). However, according to this f-test, the improvement in χ^2 by adding a power-law component has a ~1% chance of resulting from chance, and is therefore has $\lesssim 3\sigma$ significance.

To determine if the non-thermal X-ray emission reported by Combi et al. (2010) is consistent with our analysis of the significantly deeper *Suzaku* data, we used `XSpec` to simulate the expected spectrum of the foreground component and an absorbed Raymond–Smith plus power-law component with a given photon index Γ and normalization $K_{\rm PL}$, and then fit it using the Raymond–Smith model + foreground component described above. The resultant upper limit on $K_{\rm PL}$ is the highest value of $K_{\rm PL}$ for which our purely thermal model was able to fit the simulated spectrum with a reduced $\chi^2 < 2$. Since Combi et al. (2010) claim that the photon index Γ of the power-law emission varies between $\Gamma \sim 2$–3 in different regions, we determined the upper limit on $K_{\rm PL}$ for both $\Gamma = 2$ and $\Gamma = 3$. For $\Gamma = 2$, we require $K_{\rm PL} < 1.5 \times 10^{-4}$, while for $\Gamma = 3$, $K_{\rm PL} < 5 \times 10^{-4}$. Both upper limits are inconsistent with the results of Combi et al. (2010), whose fits to the southern, central, and northern regions

[10] The best fit parameters are a $N_{\rm H} = 3.3^{+0.1}_{-0.1} \times 10^{22}$ cm^{-2} and $kT = 0.80^{+0.03}_{-0.03}$ keV (errors denote the 90% confidence interval), and this fit had a $\chi^2 = 1674.91$ in 1607 degrees of freedom.

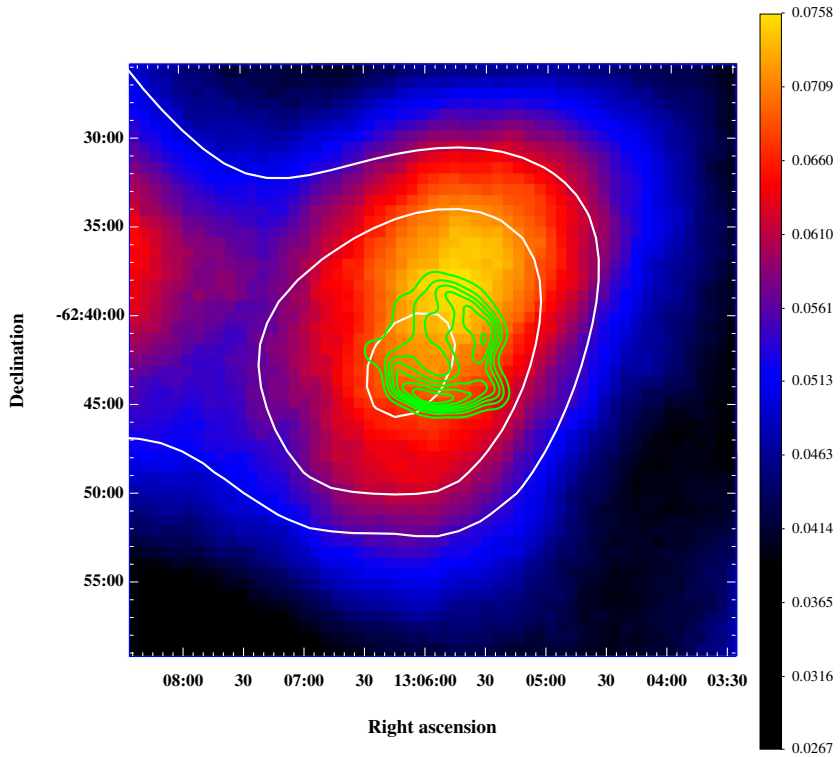

Figure 4. Smoothed *Fermi*-LAT TS map of *front* converted events in the range 2 to 200 GeV of the $0.^\circ6 \times 0.^\circ6$ region, centered on SNR Kes 17. The pixel binning is $0.^\circ01$, and the maps are smoothed with Gaussians of width $0.^\circ2$. Green contours represent the radio emission (0.843 GHz) from MOST observations. Test statistics are shown as white contours (81-100-121).

(A color version of this figure is available in the online journal.)

of Kes 17 required a combined $K_{\rm PL} \sim 10^{-3}$. Due to the fairly low statistical significance of the non-thermal component in the composite SNR spectrum extracted from the *XMM* data, and its about two to five times higher flux than allowed in the spectrum extracted from the *Suzaku* observation which detected about three times more photons from Kes 17 than *XMM*, we conclude that there is no significant non-thermal X-ray emission detected from Kes 17.

While *Suzaku* does not have the angular resolution to directly detect spatial variations in the X-ray emission of Kes 17, it is possible to use this data set to test such claims (Combi et al. 2010). If correct, modeling the observed *Suzaku* spectrum with the three absorbed `pshock` + power-law models used by Combi et al. (2010) plus the foreground component discussed above should result in a better fit than the single thermal models used above. This was not the case. However, despite having fewer degrees of freedom, the resulting fit had a χ^2 worse than the spectral fits reported in Table 2, even when we fixed the values of $N_{\rm H}$, kT, abundance, τ, and Γ of each `pshock` + power-law component to those reported by Combi et al. (2010; we allowed the normalizations to vary to account for the different size extraction regions). Therefore, we conclude that the spatial variations in the X-ray spectrum of Kes 17 reported by Combi et al. (2010) are inconsistent with the global spectrum of this remnant, and are likely the result of a combination of the different spatial and spectral resolutions of *XMM* and *Suzaku* and systematic and statistical uncertainty in the *XMM* background.

2.4. γ-Rays

Kes 17 is also detected at GeV γ-ray energies (Wu et al. 2011). To determine its properties, we analyzed 39 months (from 2008 August until 2012 February) of data collected by the *Fermi Gamma-Ray Space Telescope* Large Area Telescope (*Fermi*-LAT). We only include events belonging to the Pass 7 V6 *Source* class, which reduces the residual background rate (A. A. Abdo et al., in preparation), in this analysis. We also use the updated (Pass7 version 6; Rando & for the Fermi LAT Collaboration 2009; A. A. Abdo et al., in preparation) instrument response functions (IRFs), and reduce the contribution from terrestrial albedo γ-rays by setting a maximum zenith angle for incoming photons to 100° (Abdo et al. 2009b). We used the Fermi Science Tools v9r23p1,[11] and employed the maximum likelihood fitting technique to analyze the morphological and spectral characteristics of the γ-ray source (Mattox et al. 1996). We model the diffuse background emission in *gtlike* with a Galactic component resulting from interactions of cosmic rays with both the ISM and photons, and isotropic components accounting for extragalactic and residual backgrounds. The mapcube file `gal_2yearp7v6_v0.fits` is used to describe the γ-ray emission from the Milky Way, and the isotropic component is modeled using the `iso_p7v6source.txt` table.

The spatial characteristics of the γ-ray emission in the field of Kes 17 were studied using photons between 2 and 200 GeV converted in the *front* section of the LAT. For this subset of the γ-ray data, the 68% containment radius angle for normal incidence photons is $\leqslant 0.^\circ3$. We constructed test statistic[12] (TS) maps accounting for the Galactic and isotropic backgrounds

[11] The Science Tools package and related documentation are distributed by the Fermi Science Support Center at http://fermi.gsfc.nasa.gov/ssc.

[12] The test statistic is the logarithmic ratio of the likelihood of a point source being at a given position in a grid $L_{\rm ps}$, to the likelihood of the model without the additional source $L_{\rm null}$, $2\log(L_{\rm ps}/L_{\rm null})$.

using *gttsmap* and used this map to determine the statistical significance, position, and possible extent of the source. As shown in Figure 4, an $\sim 11.1\sigma$ (peak TS ≈ 124) unresolved (95% confidence radius $= 4'.2$) γ-ray source with centroid ($\alpha_{2000}, \delta_{2000} = 13^{\rm h}06^{\rm m}05^{\rm s}, -62^\circ 42' 54''$) is coincident with the radio emission. The residual TS map, built by modeling a point source at the best-fit centroid of emission, shows no evidence that the source is spatially extended since residual TS values are $<3\sigma$ within 1° of the centroid.

We determined the spectral energy distribution (SED) of the γ-ray source associated with Kes 17 using data from photons with energy between 0.2 and 204.8 GeV converted in both the *front* and *back* sections. We excluded photons below 200 MeV since, in this energy range, the effective area of the instrument changes rapidly and there are large uncertainties related to the Galactic diffuse model. We used *gtlike* to model the flux in each energy bin and estimated the best-fit parameters via the maximum likelihood technique. To model the background in the likelihood fits, we include sources from the 24 month *Fermi*-LAT Second Source Catalog (Nolan et al. 2012).[13] The "Pass7 version 6" IRFs we used have energy dependent systematic uncertainties in the effective area: 10% at 100 MeV, decreasing to 5% at 560 MeV, and increasing to 20% at 10 GeV (Abdo et al. 2009a; A. A. Abdo et al., in preparation and references therein). We also approximated the effect of an uncertain underlying Galactic diffuse level by artificially varying the normalization of the Galactic background by $\pm 6\%$ from the best-fit value at each energy bin, similar to the analysis of Castro & Slane (2010). As shown in Figure 5, for energies <800 MeV and >51.2 GeV only flux upper limits are determined from the data. The resultant SED is well-described by a power law with a spectral index of $\Gamma = 2.0 \pm 0.3$ and an integrated photon flux above 100 MeV of $F_{>100\,\rm MeV} \approx 1.6 \times 10^{-8}$ photons cm^{-2} s^{-1}—similar to that measured by Wu et al. (2011).

3. INTERPRETATION

As described in Section 1, by studying the broadband emission from an SNR, it is possible to determine the properties of both the material inside the remnant and in the surrounding ISM. We first analyze the non-thermal emission observed from Kes 17 to determine the physical origin of its γ-ray emission (Section 3.1), and then use those results to estimate the age of this SNR and the nature of its environment (Section 3.2). Since the shell-like radio morphology of Kes 17 suggests this emission originates at or near the forward shock (Section 2.1, Figure 1), we assume that this SNR has a radius of $R_{\rm snr} \approx 10 d_{10}$pc for a distance $d = 10 d_{10}$ kpc.

3.1. Origin of the γ-Ray Emission from Kes 17

Determining the properties of electrons and protons accelerated by this SNR requires modeling the broadband spectral characteristics of its non-thermal emission. We assume that the non-thermal radio emission is electron synchrotron radiation, while the GeV γ-ray emission is a combination of inverse-Compton (IC) scattering of ambient photons by energetic electrons, non-thermal (NT) bremsstrahlung, and the decay of π^0s produced in collisions between high energy hadrons (primarily protons) and lower energy protons.

[13] The data for the 1873 sources in the *Fermi*-LAT Second Source Catalog are made available by the Fermi Science Support Center at http://fermi.gsfc.nasa.gov/ssc/data/access/lat/2yr_catalog/.

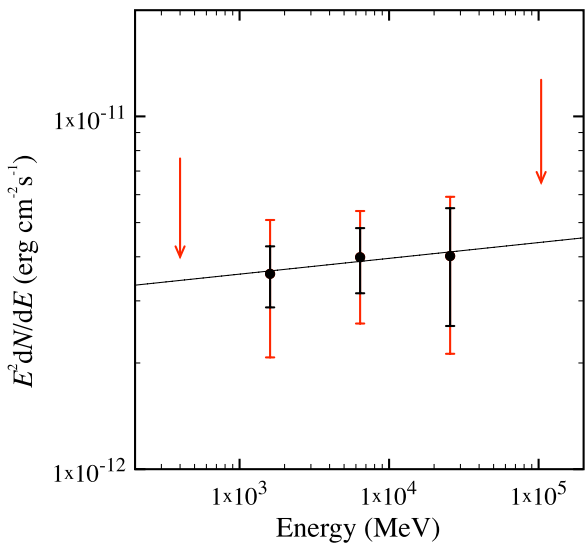

Figure 5. Spectral energy distribution of the γ-ray source coincident with Kes 17. The arrows represent the 95% confidence intervals at these energies. The black error bars represent statistical uncertainties (1σ estimates based on inverse-Hessian at the optimum of the log-likelihood surface). The red error bars represent systematic uncertainties, which are the sum in quadrature of the uncertainty related to the instrument response functions (IRFs), which we get from the instrument team (as cited in Section 2.4) and the uncertainty related to variations of the galactic diffuse background intensity, derived by changing (and fixing) the normalization of the galactic background component in the source library for the fit to 94% and 106% of the best fit value obtained from the fit to the data at a given energy bin.

(A color version of this figure is available in the online journal.)

Fitting the observed flux densities S_ν at different radio frequencies (Table 1) to a power law ($S_\nu \propto \nu^\alpha$) suggests a radio spectral index $\alpha \approx -0.6$. We further constrain our fits using the upper limits on non-thermal X-ray emission derived in Section 2.3. We consider three scenarios for the origin of the observed GeV γ-rays, each with a different dominant emission mechanism: IC emission, NT bremsstrahlung, or π^0-decay. We assume the spectral distribution $dN_{p,e}/dE$ of particles accelerated in Kes 17 is:

$$\frac{dN_{p,e}}{dE} = a_{p,e} E^{-\Gamma_{p,e}} \exp\left[-\frac{E}{E_{0\,p,e}}\right], \quad (1)$$

where $E_{0\,p,e}$ is the proton/electron energy cutoff (e.g., Reynolds 2008; Castro & Slane 2010). The electron to proton ratio at relativistic energies is given by the normalization coefficients of the distributions of these particles, $K_{ep} \equiv a_e/a_p$. These coefficients are obtained by setting the total integrated energy in accelerated particles inside the SNR shell equal to $E_{\rm cr} = \eta_{\rm cr} E_{\rm sn}$, where $\eta_{\rm cr}$ is the average efficiency of the shock in depositing energy into cosmic ray protons and $E_{\rm sn}$ is the initial kinetic energy of the supernova ejecta. In all models, we assume $E_{\rm sn} = 10^{51}$ erg, $\Gamma_p = \Gamma_e = 2.0$ (both the index predicted by basic Fermi acceleration and the value derived from fitting the observed γ-ray spectrum with a power law model; Section 2.4), and the number density of electrons $n_e = 1.23\bar{n}$ (which corresponds to material with solar abundances), where $\bar{n}$ is the volume-averaged number density of protons in the ISM surrounding Kes 17.

We model emission from π^0 decay using the work of Kamae et al. (2006), which includes a scaling factor of 1.85 for Helium and heavier nuclei (Mori 2009) as described by Castro & Slane (2010). The synchrotron and IC emission components follow

Table 3
Results from Fitting to the Broadband Spectrum of Kes 17 When Assuming Different Dominant GeV γ-Ray Emission Mechanisms

Model	K_{ep}	$\bar{n}$ (cm^{-3})	B_2 (μG)	η_{cr}	E_{0e} (TeV)	E_{0p} (TeV)	F_{IC} (10^{-9} ph cm^{-2} s^{-1})	F_{brem}	F_π
IC Dominated (A1)	0.1	1.0	10	0.6	2.2	2.2	6.2	1.5	2.6
NT Bremss. Dominated (A2)	0.5	12	15	0.08	1.5	1.5	2.9	8.9	3.2
π^0 Decay Dominated (A3)	0.01	9.0	70	0.4	0.9	30	0.3	0.8	13

Notes. K_{ep} is the electron to proton ratio at relativistic energies, $\bar{n}$ is the average density of the surrounding ISM, η_{cr} is the efficiency of cosmic ray acceleration, B_2 is the magnetic field immediately behind the shock, E_{0e} is the cut-off energy of accelerated electrons, and F_{IC}, F_{brem}, F_π are respectively the flux of inverse-Compton, non-thermal bremsstrahlung, and π^0 decay emission >100 MeV.

the models presented by (Baring et al. 1999 and references therein), and the NT bremsstrahlung emission is modeled using the prescription presented by Bykov et al. (2000). We assume the dominant photon field for IC scattering is the cosmic microwave background (CMB; $kT_{CMB} = 2.725$ K). We also assume Kes 17 is in the Sedov phase of its evolution, in which the shocked material is compressed by a factor of 4. If the swept-up material in Kes 17 is radiatively cooling, then it will be compressed by a factor $\gg$4. This with significantly increase the density of ambient cosmic ray protons swept-up by the expanding SNR, enhancing their γ-ray emission (Chevalier 1999), as well as the density of swept-up ambient cosmic ray electrons, possibly enhancing their γ-ray emission as well. However, the ages estimated in Section 3.2 suggest that this is not the case.

We built scenarios where each possible γ-ray emission mechanism (IC, NT bremsstrahlung, and π^0-decay emission) dominates by adjusting the values of K_{ep}, $\bar{n}$, E_{0e}, and the post-shock magnetic field strength B_2, and then fit the observed broadband spectrum. As shown in Figure 6, all three dominant GeV γ-ray emission mechanisms can reproduce the broadband spectrum of this SNR given the representative model parameters are listed in Table 3. However, our model requires $K_{ep} \gtrsim 0.1$ to reproduce the observed radio flux density if IC radiation (A1) or NT bremsstrahlung (A2) dominates the γ-ray emission—inconsistent with the local cosmic-ray-measured value of $K_{ep} \sim 0.01$ (Yoshida 2008). Therefore, we conclude that π^0 decay is primarily responsible for GeV γ-ray emission detected from Kes 17. Note that we assume $K_{ep} = 0.01$ for the π^0 decay scenario; similar results are obtained for lower values of η_{cr} and K_{ep} and higher values of $\bar{n}$ since $\eta_{cr} \propto \bar{n}^{-1}$ in this π^0-decay emission model (Drury et al. 1994). As a result, our modeling requires that $\bar{n} \gtrsim 9$ cm^{-3} and $\eta_{cr} \lesssim 0.4$ for π^0 decay to dominate the γ-ray emission from Kes 17.

π^0 decay is the dominant γ-ray emission mechanism even if the claims of non-thermal X-ray emission by Combi et al. (2010) or Gok & Sezer (2012) are correct. Modeling the observed broadband spectra for the non-thermal X-ray fluxes reported in these papers again requires values of K_{ep} considerably higher than measured locally if IC and/or NT bremsstrahlung emission dominate at GeV energies. These fluxes also require a higher value of E_{0e}, which subsequently changes $\bar{n}$, B_2, and η_{cr} but, due to degeneracies between these parameters, the net effect is uncertain.

Neglecting background photon fields other than the CMB (energy density $u_{CMB} = 0.260$ eV cm^{-3}) can lead us to overestimate K_{ep} when considering IC-radiation-dominated γ-ray emission. The location of Kes 17 in the Galactic plane suggests the presence of more energetic photon fields, whose inclusion would decrease the required value of K_{ep}. While IR emission is detected from Kes 17 itself (Section 2.2; Lee et al. 2011), its energy density[14] is far too low to significantly modify the value of K_{ep}.

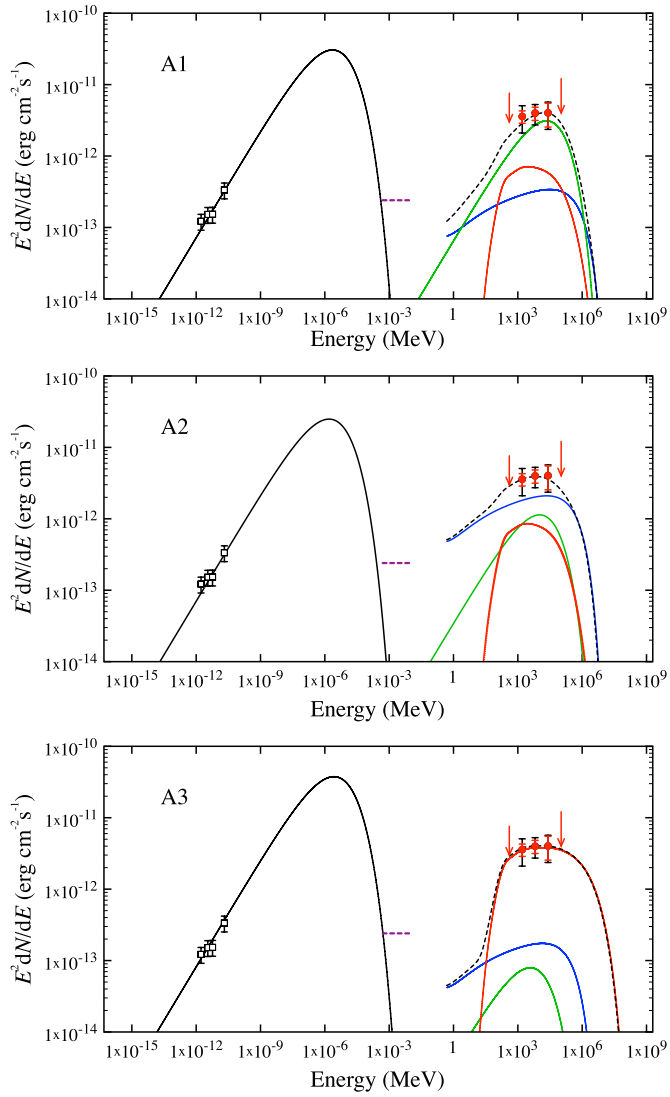

Figure 6. Broadband fits to radio (open squares; Shaver & Goss 1970; Whiteoak & Green 1996, and *Fermi*-LAT (red circles) observations of Kes 17 with the A1 (top), A2 (middle), and A3 (bottom) models. The modeled spectra from synchrotron emission (black), inverse Compton emission (green), π^0-decay (red), and non-thermal bremsstrahlung (blue), are shown. The dashed purple line indicates the upper limit for non-thermal X-ray emission determined from the *Suzaku* observations, using a power-law model with index $\Gamma = 2$.

(A color version of this figure is available in the online journal.)

[14] We calculate $u \sim 8 \times 10^{-4}$ eV cm^{-3} for the $T \approx 79$ K, $L \approx 1500$ $L_\odot$ modified blackbody and $u \sim 6.5 \times 10^{-3}$ eV cm^{-3} for $T \approx 27$ K, $L \approx 12500$ $L_\odot$ modified blackbody.

Table 4
The Physical Properties of SNRs Other Than Kes 17 with Direct Observational Evidence for Proton Acceleration

SNR	Age	$\bar{n}$	ISM	$B_{\rm snr}$	$\eta_{\rm cr}$	$K_{\rm ep}$	$E_{0,p}$	Citations
Kes 17	∼2,000–40,000	>9 cm^{-3}	Clumpy	35 μG	<0.4	0.02	>500 GeV	···
Cas A	330 yr	30 cm^{-3}	Clumpy	0.5–1 mG	0.005–0.02	0.004–0.02	10–30 TeV	[a, b, c, v]
Tycho	440 yr	∼0.3 cm^{-3}	Uniform	200–300 μG	0.06–0.075	0.0016	>470 TeV	[h, i, j, k]
IC 443	4,000 yr	∼250 cm^{-3}	Clumpy	10 μG	0.006–0.02	0.01–0.03	100–200 GeV	[d, e, f, g]
W44	20,000 yr	∼100 cm^{-3}	Clumpy	40–800 μG	0.03–0.15	0.01–0.05	···	[n, o, p, q, g, r]
W51C	30,000 yr	10 cm^{-3}	Clumpy	<150 μG	0.16	0.0125	120 TeV	[s, t, g, u]
W28	40,000 yr	$\gtrsim$100 cm^{-3}	Clumpy	40–160 μG	0.01–0.03	0.01	···	[l, m, g]

Notes. $\bar{n}$ is the average density of the surrounding ISM, $B_{\rm snr}$ is the strength of the magnetic field inside the SNR, $\eta_{\rm cr}$ is the ratio between $E_{\rm cosmicray}$ and the initial kinetic energy of the progenitor SN (assumed in many cases to be 10^{51} erg), K_{ep} is the relative normalization between accelerated electrons and positrons, and $E_{0,p}$ is the cutoff energy in the acceleration proton spectrum. Ranges given for various values reflect differences in the literature, and for some SNRs the reported values are assumptions used in the modeling as opposed to fitted values. No value for $E_{0,p}$ is given for SNRs W28 and W44 since a broken power-law cosmic-ray injection spectrum, as opposed to a power-law with an exponential cutoff, is needed to reproduce their non-thermal spectra. [a] Berezhko et al. (2003). [b] Berezhko & Völk (2004). [c] Abdo et al. (2010a). [d] Troja et al. (2008). [e] Abdo et al. (2010d). [f] Tavani et al. (2010). [g] Tang et al. (2011). [h] Cassam-Chenaï et al. (2007). [i] Eriksen et al. (2011). [j] Giordano et al. (2012). [k] Morlino & Caprioli (2012). [l] Abdo et al. (2010b). [m] Giuliani et al. (2010). [n] Reach et al. (2005). [o] Abdo et al. (2010c). [p] Uchiyama et al. (2010). [q] Giuliani et al. (2011). [r] Uchiyama et al. (2012). [s] Koo et al. (1995). [t] Koo et al. (2010). [u] Aleksić et al. (2012). [v] Kim et al. (2008).

Other possible photon fields are ambient starlight ($T \sim 5000$ K) and emission from warm dust ($T \sim 25$ K). To determine if they could allow IC to dominate the observed γ-rays, we estimate the photon energy density required for IC scattering of relativistic electrons in the SNR off these photons to be primarily responsible for the bulk of the γ-ray emission if $K_{\rm ep} = 0.01$. Since the required photon energy density decreases for larger energy in relativistic electrons $E_{\rm elec}$, we use the maximum electron energy allowed by the data. A cosmic ray acceleration efficiency $\eta = 0.4$ (as suggested by the π^0 decay model) suggests $E_{\rm cr} = 0.4 \times 10^{51}$ erg. For $K_{\rm ep} = 0.01$ and the electron cut off energies given in Table 3, the total energy in relativistic electrons is $E_{\rm elec} = 3.4 \times 10^{48}$ erg. By choosing such a high cosmic ray acceleration efficiency, we likely overestimate the true energy in relativistic electrons, and therefore our analysis *underestimates* the required energy density.

If the background photons are dominated by emission from warm dust, it must have an energy density $u_{\rm dust} \gtrsim 40 u_{\rm CMB}$. If the background photons are dominated by starlight, it must have an energy density $u_{\rm starlight} \gtrsim 500 u_{\rm CMB}$. Since a combination of the two is likely, we also fit for the required energy density of starlight assuming $u_{\rm dust} = 20 u_{\rm CMB}$. In this case, the required $u_{\rm starlight} \gtrsim 200 u_{\rm CMB}$. In each scenario, the required energy density of both dust emission and starlight is significantly higher than the values estimated from modeling the observed diffuse γ-ray emission of the Milky Way (Strong et al. 2000). As a result, photons from starlight and warm dust incident on Kes 17 are unlikely to have the high energy densities needed for IC emission to be the dominant γ-ray emission mechanism. Therefore, we conclude that π^0 decay is likely responsible for the bulk of the γ-ray emission observed from Kes 17.

If correct, then Kes 17 is one of few ($\lesssim$10) SNRs with direct observational evidence for acceleration protons to high energies. In Table 4, we compare the physical properties of Kes 17 with those other such remnants. For many of these SNRs, the broadband spectral modeling also assume that $K_{ep} \sim 0.01$. Due to the lack of spectral information at TeV energies, we can only constrain $E_{0p} > 500$ GeV for Kes 17 (Table 3)—higher than the observed value for SNR IC 443, but consistent with the measured value of other SNRs (Table 4). The strength of the post-shock magnetic field, $B_{\rm snr}$, is also within the range spanned by cosmic-ray producing SNRs—though closer to the value inferred for the older ($t_{\rm age} \gtrsim 4000$ yr) SNRs (e.g., IC 443, W51C, W28) than the younger ($t_{\rm age} < 1000$ yr) SNRs (e.g., Cas A and Tycho's SNR) among this group. The allowed average density $\bar{n}$ is within the range spanned by this group, though the average cosmic-ray acceleration efficiency $\eta_{\rm cr}$ required for the lowest allowed value of $\bar{n}$ is quite high: roughly five times higher than that of the younger SNRs and about two times higher than any of the older cosmic-ray producing SNRs. Only by determining the physical properties of the environment surrounding Kes 17, as we do in Section 3.2, can we determine if this SNR is an especially efficient producer of cosmic rays.

3.2. Environment of Kes 17

As discussed in Section 3.1, a primarily hadronic origin for the GeV γ-rays detected from Kes 17 requires this SNR to expand into an ISM with a volume-averaged density of $\bar{n} \gtrsim 9(\eta_{\rm cr}/0.4)^{-1}$ cm^{-3} (Section 3.1, Table 3). In this section, we wish to determine if this environment is consistent with the radius (Section 2.1), dust mass (Section 2.2), and electron temperature (Section 2.3) observed from this remnant. This analysis also allows us to infer the basic properties, e.g., its age $t_{\rm age}$ and current expansion velocity $v_{\rm snr}$, needed to understand the underlying particle acceleration mechanism (e.g., Reynolds & Keohane 1999; Reynolds 2008).

The $\gtrsim$3–11 $M_\odot$ of dust in the SNR shell inferred from IR observations (Section 2.2; Lee et al. 2011) is likely dominated by pre-existing dust swept up by the expanding ejecta or dust formed inside the remnant. If Kes 17 is expanding into a medium with a volume average density $\bar{n} = 10\bar{n}_{10}$ cm^{-3} (where $\bar{n}_{10} \gtrsim 1$, Section 3.1), then the mass of material swept-up by the expanding supernova ejecta $M_{\rm sw}$ is:

$$M_{\rm sw} = \frac{4}{3}\pi R_{\rm snr}^3 \bar{n} m_{\rm p} \quad (2)$$

$$\approx 1300 \bar{n}_{10} d_{10}^3 \, M_\odot. \quad (3)$$

If this medium has a typical dust-to-gas mass ratio of ∼0.1%–0.5% (e.g., Pei 1992), then Kes 17 has swept-up $\sim (1-5)\bar{n}_{10}$ $M_\odot$ of interstellar dust, comparable to the mass

estimated from observations. If there is considerably more mass at lower temperatures (Lee et al. 2011), this does not indicate that the additional dust was formed inside the SNR, but likely indicates $\bar{n}_{10} > 1$ and/or a higher dust-to-gas mass ratio in the surrounding medium, which is possible if Kes 17 is expanding into a molecular cloud. In fact, the detection of OH (1720 MHz) maser (Section 2.1) and molecular shock (Section 2.2) emission indicates this SNR is expanding inside a molecular cloud (Yusef-Zadeh et al. 2003). This implies that the clumps observed in the IR are likely the result of dense material inside the cloud swept-up and shocked by the expanding ejecta (Section 2.2).

While molecular clouds have a very complicated density structure (e.g., Williams et al. 1995), one can approximate this environment as a collection of clumps with an average density $\bar{n}_{\rm clump}$ and volume filling factor $f_{\rm clump}$ embedded in a uniform interclump medium with a density $n_{\rm ic}$ and volume filling factor $1 - f_{\rm clump}$ (Chevalier 1999). In this model, $\bar{n}$ is

$$\bar{n} = \bar{n}_{\rm clump} f_{\rm clump} + n_{\rm ic}(1 - f_{\rm clump}). \quad (4)$$

As noted in Section 3.1, the acceleration efficiency $\eta_{\rm cr} \propto \bar{n}^{-1}$, and $\eta_{\rm cr} \sim 10\%$ (the value inferred for other remnants; Table 4) requires $\bar{n} \sim 90$ cm^{-3}. These parameters ($\bar{n}$, $n_{\rm ic}$, $\bar{n}_{\rm clump}$, $f_{\rm clump}$) have been measured for a few molecular clouds, which find that typically $n_{\rm ic} \lesssim 10$ cm^{-3}, $f_{\rm clump} \sim 10\%$, $\bar{n} \sim 20$ cm^{-3}, and $\bar{n}_{\rm clump} \sim$ 200–1000 cm^{-3} with considerable variation between clouds (e.g., Blitz 1993; Williams et al. 1995). From the analysis of the thermal X-ray spectrum of Kes 17 presented in Sections 3.2.1 and 3.2.2, we estimate $n_{\rm ic} \lesssim 0.4$ cm^{-3}. If $\bar{n} \sim 9$ cm^{-3}, $\bar{n}_{\rm clump} = 200$ cm^{-3}, and $n_{\rm ic} \sim 0.4$ cm^{-3}, then $f_{\rm clump} \sim 4\%$—consistent with the observed values. However, if $\bar{n} \sim 90$ cm^{-3}, then $f_{\rm clump}$ is an extremely high ∼45% for these values of $\bar{n}_{\rm clump}$ and $n_{\rm ic}$. But, if $\bar{n}_{\rm clump} \sim 1000$ cm^{-3}, as measured around HII region NGC 2244 which is inside a molecular cloud (Williams et al. 1995), then $f_{\rm clump} \sim 10\%$ for $\bar{n} \sim 90$ cm^{-3} and $n_{\rm ic} \sim 0.4$ cm^{-3}. The range of clump densities ($n_{\rm clump} \sim$ 100–1000 cm^{-3} up to $n \sim 10^4$–10^6 cm^{-3}) inferred from analysis of the IR spectrum of Kes 17 (Section 2.2) suggests $\bar{n}_{\rm clump} \sim 1000$ cm^{-3} is plausible.

Interpreting the radius and X-ray temperature of Kes 17 requires understanding its dynamical evolution. A supernova ejects material of mass $M_{\rm ej}$ and initial kinetic energy $E_{\rm sn}$ into its surroundings. Initially, the ejecta expands supersonically relative to its environment, driving a shock called the "forward shock" into its surroundings. At this shock, the swept-up ambient material is accelerated, compressed, and heated to a pressure significantly higher than that of the expanding ejecta. As a result, the shocked ambient material drives a shock wave, called the "reverse shock," into the expanding ejecta which decelerates, compresses, and heats this material. In the standard evolutionary model for SNRs (e.g., Chevalier 1977; Truelove & McKee 1999 and references therein), at early times the forward shock expands with a roughly constant velocity, such that the radius of the forward shock $R_{\rm snr} \propto t$. Since it expands with constant velocity, the ejecta lose little kinetic energy during this phase. This "free expansion" phase ends when the reverse shock has passed through all of the ejecta, approximately when the mass swept-up by the forward shock $M_{\rm sw} \approx M_{\rm ej}$. During this phase, commonly referred to as the "Sedov-Taylor phase," adiabatic losses are expected to dominate the energy evolution of the ejecta, and the SNR expands as $R_{\rm snr} \propto t^{2/5}$ (e.g., Chevalier 1977; Truelove & McKee 1999 and references therein). When the radiative cooling time of the shocked gas is comparable to the age of the SNR, radiative losses dominate, significantly changing its dynamical evolution (Blondin et al. 1998).

However, the evolution of Kes 17 will be significantly different due to its expansion into a clumpy molecular cloud (e.g., Chevalier 1999) and its efficient acceleration of cosmic rays (e.g., Ellison et al. 2007, 2010; Ferrand et al. 2010; Castro et al. 2011). Observational evidence that Kes 17 has evolved differently is its "mixed morphology" nature (Combi et al. 2010), defined by the observed combination of steep-spectrum radio shell and interior thermal X-ray emission (Rho & Petre 1998). The non-Sedov density and temperature profile suggested by its center-filled thermal X-ray morphology can modify the growth of the SNR (e.g., White & Long 1991). Currently, the two leading physical explanations for mixed-morphology SNRs are that thermal conduction drives gas heated at the forward shock to the center (e.g., Cui & Cox 1992; Chevalier 1999) or that dense clumps are evaporating inside the remnant (e.g., White & Long 1991). While neither model accurately reproduces the observed temperature and X-ray surface brightness profiles of all mixed-morphology SNRs (e.g., Slane et al. 2002), we will interpret the radius of electron temperature of Kes 17 using these models to roughly estimate its age and environment.

3.2.1. Thermal Conduction

If heat conduction is primarily responsible for the thermal X-rays observed in the center of Kes 17, then its evolution is likely similar to the "standard" sequence outlined above. As before, we approximate the molecular cloud environment as a collection of discrete, small, high density clumps embedded in low, constant density interclump gas (Chevalier 1999). The expanding ejecta will shock both the interclump gas and the clumps, but, for the clump densities inferred from IR observations ($n_{\rm clump} \sim 10^2$–10^6 cm^{-3}; Section 2.2), the transmitted shock is too slow to heat this material to X-ray emitting temperatures. Therefore, the mass of the X-ray emitting gas in Kes 17 M_X should not exceed the mass of swept-up interclump material $M_{\rm ic}$ ($M_X \leqslant M_{\rm ic}$).

It is possible to estimate M_X from the fits to thermal X-ray spectrum presented in Section 2.3. The mass of the X-ray emitting gas is equal to:

$$M_X = \frac{4}{3}\pi R_{\rm snr}^3 f_X n_{H,X} m_p, \quad (5)$$

where m_p is the mass of the proton, $n_{H,X}$ is the density of the X-ray emitting gas, and f_X is the fraction of the SNR's volume filled with the X-ray emitting plasma. We can estimate $n_{H,X}$ from the normalization K of the thermal X-ray emission models used in Section 2.3, since (Arnaud 1996):

$$K = \frac{10^{-14}}{4\pi d^2} \int n_{e,X} n_{H,X} dV \quad (6)$$

$$= 0.3 f_X \mu^{-1} n_{H,X}^2 d\theta_{\rm snr}^3 \times 10^{-14} \quad (7)$$

where μ is the number ratio of electrons to protons in the plasma ($n_{H,X} = n_{e,X}/\mu$; $\mu = 1.23$ for solar abundance), d is the distance to the source in cm, and $\theta_{\rm snr}$ is the angular radius of Kes 17 in radians. For the measured values of K (Table 2, Section 2.3), $n_{H,X}$ is approximately:

$$n_{H,X} \sim 0.4 f_X^{-\frac{1}{2}} d_{10}^{-\frac{1}{2}} \text{ cm}^{-3}. \quad (8)$$

For a standard SNR, $f_X \approx 1/12$, but a mixed morphology SNR likely has f_X greater than this value. Since $1/12 \leqslant f_X \leqslant 1$, we therefore estimate:

$$n_{H,X} \sim (0.4 - 1.4) d_{10}^{-\frac{1}{2}}\ \mathrm{cm}^{-3}. \tag{9}$$

Relating M_X to $M_{\rm ic}$ requires estimating the cooling time of the X-ray emitting gas $t_{\rm cool}$. If Kes 17 is significantly older than the cooling time, then $M_X \ll M_{\rm ic}$, while if Kes 17 is younger than the cooling time, then $M_X \approx M_{\rm ic}$. The cooling time can be approximated as

$$t_{\rm cool} \approx \frac{E_{\rm thermal}}{L_{\rm thermal}}, \tag{10}$$

where $E_{\rm thermal}$ is the thermal energy of this gas and $L_{\rm thermal}$ is its thermal luminosity. The thermal energy is roughly

$$E_{\rm thermal} = \frac{4}{3}\pi R_{\rm snr}^3 n_{H,X} f_X k_B T_X, \tag{11}$$

where k_B is Boltzmann's constant and T_X is the X-ray temperature, while the thermal luminosity $L_{\rm thermal}$ is

$$L_{\rm thermal} = \frac{4}{3}\pi R_{\rm snr}^3 \Lambda \tag{12}$$

where, for solar abundances and temperature $kT_X \sim 1$ keV (the average electron temperature and approximate chemical composition suggested by our modeling; Section 2.3), Λ is (Raymond et al. 1976)

$$\Lambda \sim 5 n_{\rm e,X} n_{\rm H,X} \times 10^{-23}\ \mathrm{erg\ s^{-1}\ cm^{-3}} \tag{13}$$

$$\sim 5 \mu n_{\rm H,X}^2 \times 10^{-23}\ \mathrm{erg\ s^{-1}\ cm^{-3}}. \tag{14}$$

This suggests that:

$$t_{\rm cool} \approx \frac{k_B T_x f_X}{5 \mu n_{H,x} \times 10^{-23}} \tag{15}$$

$$\approx 2 f_X^{\frac{1}{2}} \times 10^6\ \mathrm{yr} \tag{16}$$

$$\sim (0.6\text{–}2) \times 10^6\ \mathrm{yr} \tag{17}$$

for the range of f_X argued above. This is considerably higher than the age of the other SNRs identified as efficient cosmic ray accelerators (Table 4). Therefore, in this scenario, it is likely that $M_X \approx M_{\rm ic}$.

The mass of the interclump gas swept-up by the expanding ejecta is

$$M_{\rm ic} = \frac{4}{3}\pi R_{\rm snr}^3 (1 - f_{\rm clump}) n_{\rm ic} m_p. \tag{18}$$

For $M_X \approx M_{\rm ic}$, we have

$$n_{\rm ic} \approx \frac{f_X}{1 - f_{\rm clump}} n_{H,X} \tag{19}$$

$$\approx 0.4 f_X^{\frac{1}{2}} (1 - f_{\rm clump})^{-1} d_{10}^{-\frac{1}{2}}\ \mathrm{cm}^{-3}. \tag{20}$$

If $f_{\rm clump} \sim 10\%$, as suggested by observations (e.g., Blitz 1993; Williams et al. 1995), the allowed range of f_X favors $n_{\rm ic} \sim 0.1$–$0.4\ \mathrm{cm}^{-3}$.

As mentioned above, in this scenario the evolution of Kes 17 should be similar to that of the "standard" SNR. Therefore, its observed radius $R_{\rm snr}$ suggests an age (e.g., Lozinskaya 1992):

$$t_{\rm age} = \left(\frac{R_{\rm snr}}{1.15}\right)^{\frac{5}{2}} \left(\frac{n_{\rm ic} \mu m_{\rm p}}{E_{\rm sn}}\right)^{\frac{1}{2}} \tag{21}$$

$$\approx 4200 d_{10}^{\frac{5}{2}} \left(\frac{n_{\rm ic}}{0.4}\right)^{\frac{1}{2}} E_{51}^{-\frac{1}{2}}\ \mathrm{yr}, \tag{22}$$

where $E_{\rm sn} = 10^{51} E_{51}$ erg. For the values of $n_{\rm ic}$ estimated above, Kes 17 is only $t_{\rm age} \sim 2000$–4200 yr old. This is considerably lower than the cooling timescale $t_{\rm cool}$ calculated above, consistent with our assumption that $M_X \approx M_{\rm ic}$. While this age estimate ignores the effect of cosmic ray acceleration, numerical studies suggest that this analysis underestimates the age by ~20% in the case of extremely efficient particle acceleration ($\eta_{\rm cr} \sim 40\%$; e.g., Castro et al. 2011). Therefore, in this scenario we estimate that Kes 17 is $t_{\rm age} \sim 2000$–5200 yr old.

If correct, Kes 17 is currently expanding with a speed $v_{\rm snr}$ (e.g., Lozinskaya 1992; Truelove & McKee 1999):

$$v_{\rm snr} \approx 0.43 \left(\frac{E_{\rm sn}}{n_{\rm ic} m_{\rm p}}\right)^{\frac{1}{2}} R_{\rm snr}^{-\frac{3}{2}} \tag{23}$$

$$\sim 570 \left(\frac{n_{\rm ic}}{\mathrm{cm}^{-3}}\right)^{-\frac{1}{2}} \frac{\mathrm{km}}{\mathrm{s}}. \tag{24}$$

If $n_{\rm ic} \sim 0.1$–$0.4\ \mathrm{cm}^{-3}$ as derived above, then $v_{\rm snr} \sim 900$–$1800\ \mathrm{km\ s^{-1}}$. Such a shock is expected to heat electrons to a temperature T_e

$$kT_e \approx \frac{3}{16} m_e v_{\rm snr}^2 \tag{25}$$

$$\sim 0.9\text{–}3\ \mathrm{eV}, \tag{26}$$

substantially lower than the $kT_e \sim 0.8$ keV inferred from our modeling of the observed X-ray spectrum (Section 2.3). However, ions are heated to a temperature T_i

$$kT_i \approx \frac{3}{16} m_p v_{\rm snr}^2 \tag{27}$$

$$\sim 1.5\text{–}6\ \mathrm{keV}, \tag{28}$$

higher than the observed electron temperature. However, many electron heating mechanisms operate inside an SNR. Observations suggest that, at a forward shock expanding with $v_{\rm snr} \sim 900$–$1800\ \mathrm{km\ s^{-1}}$, electrons will be heated to a temperature of $T_e \sim (0.1\text{–}0.8) T_i$ at the forward shock for this range of shock velocities (Ghavamian et al. 2007), with this process possibly enhanced by efficient particle acceleration at the forward shock (Castro et al. 2011). Additionally, inside the SNR, ions heat the electrons through Coulomb collisions. The high ionization timescale inferred from our modeling of the observed thermal

X-ray spectrum suggests at least rough thermal equilibration between electrons and ions in this remnant. Therefore, this scenario is consistent with the observed electron temperature.

In summary, if thermal conduction is the dominant mechanism responsible for the mixed morphology nature of Kes 17, then this remnant is ∼2000–5000 yr old and is expanding into a clumpy medium with an interclump density of ∼0.1–0.4 cm^{-3}.

3.2.2. Clump Evaporation

Alternatively, the mixed morphology nature of Kes 17 could result from dense clumps swept up by the expanding ejecta evaporating inside the remnant and then being heated to X-ray temperatures by the hot interclump gas shocked at the forward shock. In this case, we expect $M_X > M_{\rm ic}$. Repeating the analysis of Section 3.2.1, this requires that

$$n_{\rm ic} \lesssim 0.4 f_X^{\frac{1}{2}} (1 - f_{\rm clump})^{-1} d_{10}^{-\frac{1}{2}}\ {\rm cm}^{-3}. \quad (29)$$

Since $f_X < 1$, in this scenario $n_{\rm ic} < 0.4$ cm^{-3}.

The evaporation of clumps inside the SNR can significantly impact the dynamics of the forward shock, which is now expected to expand as

$$R_{\rm snr} = \left[\frac{25(\gamma+1)\kappa E_{\rm sn}}{16\pi n_{\rm ic} m_{\rm p}}\right]^{\frac{1}{5}} t^{\frac{2}{5}}, \quad (30)$$

where $\gamma = 5/3$ is the adiabatic index of the surrounding material and κ is the ratio of thermal to kinetic energy in the SNR (White & Long 1991). Therefore, the age of Kes 17 is

$$t_{\rm age} = \left[\frac{25(\gamma+1)}{16\pi m_{\rm p}}\right]^{-\frac{1}{2}} \left(\frac{\kappa E_{\rm sn}}{n_{\rm ic}}\right)^{-\frac{1}{2}} R_{\rm snr}^{\frac{5}{2}} \quad (31)$$

$$\approx 6000 \kappa^{-\frac{1}{2}} E_{51}^{-\frac{1}{2}} n_{\rm ic}^{\frac{1}{2}}\ {\rm yr} \quad (32)$$

for $d_{10} = 1$, where κ can vary between 0.01 and 1 (White & Long 1991). Setting $\kappa = 0.01$ and $n_{\rm ic} = 0.4$ cm^{-3} suggests that $t_{\rm age} < 40000$ yr old. While this analysis ignores the effect of efficient particle acceleration on the evolution of the forward shock (White & Long 1991), the resulting ∼20% error suggested by simulations (e.g., Castro et al. 2011) is considerably less than the uncertainty resulting from the unknown values of κ and $n_{\rm ic}$.

In this scenario, $v_{\rm snr}$ is given by:

$$v_{\rm snr} = \frac{2}{5}\left[\frac{25(\gamma+1)\kappa E_{\rm sn}}{16\pi n_{\rm ic} m_{\rm p}}\right]^{\frac{1}{5}} t_{\rm age}^{-\frac{3}{5}}, \quad (33)$$

$$\approx 120,000 \left(\frac{\kappa E_{51}}{n_{\rm ic}}\right)^{\frac{1}{5}} \left(\frac{t_{\rm age}}{1\ {\rm yr}}\right)^{-\frac{3}{5}} \frac{\rm km}{\rm s}. \quad (34)$$

By considering the "maximum age" case above ($\kappa = 0.01$, $n_{\rm ic} = 0.4$ cm^{-3}, and $t_{\rm age} = 40000$ yr), we find that currently $v_{\rm snr} \geqslant 100$ km s^{-1}. From Equations (25) and (27), this minimum velocity is too slow to currently heat either electrons or ions to the measured electron temperature $kT_e \sim 0.8$ keV (Section 2.3). This can be rectified by Kes 17 either being younger than the maximum age estimated above, suggesting $\kappa > 0.01$ and/or $n_{\rm ic} < 0.4$ cm^{-3}, or the emitting material was heated at an earlier time when the SNR was expanding faster. This is plausible since the time required for the X-ray emitting gas to cool ($t_{\rm cool} \gtrsim 6 \times 10^5$ yr; Section 3.2.1, Equation (15)) is longer than the maximum age of Kes 17 in this scenario. Therefore, it is plausible that material heated at earlier times would still radiate today.

In summary, if clump evaporation is the dominant cause of the mixed morphology nature of Kes 17, it is expanding into a medium with an interclump density $n_{\rm ic} < 0.4$ cm^{-3} and is <40000 yr old.

4. CONCLUSIONS

In this paper, we analyze and interpret recent observations of SNR Kes 17 across the electromagnetic spectrum (Section 2). Our analysis indicates this SNR has a partial radio shell with a diameter of ∼7′.5, which translates to a physical radius of $R \sim 10 d_{10}$ pc at a distance $d = 10 d_{10}$ kpc. The detection of OH 1720 MHz maser emission and the IR spectrum of Kes 17 suggest that this SNR is expanding into a molecular cloud, and our analysis of a recent *Suzaku* observation of this SNR suggests the observed X-ray emission is predominantly thermal, emitted by a plasma with a density of $n_{H,X} \sim 0.4$ cm^{-3}, roughly solar abundances except for an under-abundance of S, and comprised of gas with an electron temperature $kT_{\rm e} \approx 0.8$ keV in roughly thermal equilibrium (Sections 2.3 and 3.2; Table 2). Finally, our analysis of *Fermi* observations of this field strongly detects GeV γ-ray emission coincident with this remnant that is almost certainly from the SNR shell (Section 2.4).

By modeling the broadband non-thermal emission of Kes 17, we determined that the GeV γ-rays are predominantly the result of cosmic ray protons accelerated at the SNR's forward shock colliding with swept-up material inside the SNR, producing π^0's that decay into γ-rays (Section 3.1). This explanation requires that this SNR is expanding into medium with an average density $\bar{n} \gtrsim 9$ cm^{-3} (Section 3.1), consistent with the molecular cloud environment implied by the OH maser emission and considerable dust mass inferred from its IR spectrum (Section 3.2). The age of Kes 17 and density of the interclump medium inside the cloud $n_{\rm ic}$ depends on whether thermal conduction or evaporation of dense clumps is primarily responsible for the mixed morphology nature of this remnant. If thermal conduction is responsible, then Kes 17 is expanding into an environment with $n_{\rm ic} \sim 0.1$–0.4 cm^{-3} and is only ∼2000–5000 yr old (Section 3.2.1). However, if the evaporation of density clumps is primarily responsible, then Kes 17 is expanding inside an environment with $n_{\rm ic} < 0.4$ cm^{-3} and can be as much as ∼40000 yr old (Section 3.2.2). If the cosmic ray efficiency $\eta_{\rm cr}$ of Kes 17 is similar to that other SNRs believed to be accelerating cosmic rays (Table 4), then it is expanding in an environment with $\bar{n} \sim 90$ cm^{-3} (Section 3.2). This requires the surrounding clumps have an average density of $\bar{n}_{\rm clump} \sim 1000$ cm^{-3} for a reasonable clump mass fraction of $f_{\rm clump} \sim 10\%$ (Section 3.2). Such an average clump density has been observed in some molecular clouds (Blitz 1993) as well around massive stars which have formed a stellar wind bubble or HII inside a molecular cloud (Williams et al. 1995).

The possible high cosmic ray acceleration efficiency inferred in Kes 17 is very interesting—especially given its likely expansion into a clumpy medium. Much about the particle acceleration mechanism inside SNRs, particularly how its efficiency depends on its surroundings, is unknown. Recent theoretical work suggests that expansion into a turbulent, clumpy, strongly magnetized environment enhances cosmic ray acceleration (e.g., Bykov et al. 2000; Zhang et al. 2009), and further study of Kes

17 would test these results. This requires better understanding the environment of Kes 17, specifically the clumpiness of its surroundings. Additional observations are also needed to measure the properties of the accelerated cosmic rays in order to test models of the acceleration mechanism. This can be accomplished in a variety of ways, e.g., measuring the TeV γ-ray spectrum will allow us to determine the maximum energy of cosmic rays accelerated in the SNR E_{0p}, mapping CO emission around Kes 17 will allow us to measure the average density $\bar{n}$ of its environment (e.g., Williams et al. 1995), and a deeper X-ray observation will allow us use the observed thermal X-ray emission (e.g., Ellison et al. 2010) to constrain the cosmic ray acceleration efficiency $\eta_{\rm cr}$, better constrain the energetics of any cosmic ray electrons accelerated in this SNR, and determine the origin of its mixed morphology appearance. In any case, future study of Kes 17 is extremely important for understanding how energetic particles are accelerated in SNRs.

The authors thank the anonymous referee for usual comments and suggestions. J.D.G. acknowledges the support of NASA grant NNX10AR51G, and NSF Astronomy and Astrophysics Postdoctoral Fellowship grant AST-0702957, as well as the hospitality of the Center for Cosmology and Particle Physics at New York University where much of this work was conducted. P.O.S. acknowledges support from NASA contract NAS8-03060. The Australia Telescope is funded by the Commonwealth of Australia for operation as a National Facility managed by CSIRO. This research has made use of data obtained from the *Suzaku* satellite, a collaborative mission between the space agencies of Japan (JAXA) and the USA (NASA).

REFERENCES

Abdo, A. A., Ackermann, M., Ajello, M., et al. 2009a, PhRvL, 103, 251101
Abdo, A. A., Ackermann, M., Ajello, M., et al. 2009b, PhRvD, 80, 122004
Abdo, A. A., Ackermann, M., Ajello, M., et al. 2010a, ApJL, 710, L92
Abdo, A. A., Ackermann, M., Ajello, M., et al. 2010b, ApJ, 718, 348
Abdo, A. A., Ackermann, M., Ajello, M., et al. 2010c, Sci, 327, 1103
Abdo, A. A., Ackermann, M., Ajello, M., et al. 2010d, ApJ, 712, 459
Ackermann, M., Ajello, M., Allafort, A., et al. 2013, Sci, 339, 807
Aleksić, J., Alvarez, E. A., Antonelli, L. A., et al. 2012, A&A, 541, A13
Anders, E., & Grevesse, N. 1989, GeCoA, 53, 197
Arendt, R. G. 1989, ApJS, 70, 181
Arnaud, K. A. 1996, in ASP Conf. Ser. 101, Astronomical Data Analysis Software and Systems V, ed. G. H. Jacoby & J. Barnes (San Francisco, CA: ASP), 17
Arnett, W. D., & Schramm, D. N. 1973, ApJL, 184, L47
Baring, M. G., Ellison, D. C., Reynolds, S. P., et al. 1999, ApJ, 513, 311
Berezhko, E. G., Pühlhofer, G., & Völk, H. J. 2003, A&A, 400, 971
Berezhko, E. G., & Völk, H. J. 2004, A&A, 419, L27
Blackburn, J. K. 1995, in ASP Conf. Ser. 77, Astronomical Data Analysis Software and Systems IV, ed. R. A. Shaw, H. E. Payne, & J. J. E. Hayes (San Francisco, CA: ASP), 367
Blitz, L. 1993, in Protostars and Planets III, ed. E. H. Levy & J. I. Lunine (Tucson, AZ: Univ. Arizona Press), 125
Blondin, J. M., Wright, E. B., Borkowski, K. J., et al. 1998, ApJ, 500, 342
Bykov, A. M., Chevalier, R. A., Ellison, D. C., et al. 2000, ApJ, 538, 203
Cassam-Chenaï, G., Hughes, J. P., Ballet, J., et al. 2007, ApJ, 665, 315
Castro, D., & Slane, P. 2010, ApJ, 717, 372
Castro, D., Slane, P., Patnaude, D. J., et al. 2011, ApJ, 734, 85
Caswell, J. L., Murray, J. D., Roger, R. S., et al. 1975, A&A, 45, 239
Chevalier, R. A. 1977, ARA&A, 15, 175
Chevalier, R. A. 1999, ApJ, 511, 798
Combi, J. A., Albacete Colombo, J. F., Sánchez-Ayaso, E., et al. 2010, A&A, 523, A76
Cui, W., & Cox, D. P. 1992, ApJ, 401, 206
Drury, L. O., Aharonian, F. A., & Voelk, H. J. 1994, A&A, 287, 959
Elitzur, M. 1976, ApJ, 203, 124
Ellison, D. C., Patnaude, D. J., Slane, P., et al. 2007, ApJ, 661, 879
Ellison, D. C., Patnaude, D. J., Slane, P., et al. 2010, ApJ, 712, 287
Eriksen, K. A., Hughes, J. P., Badenes, C., et al. 2011, ApJL, 728, L28
Ferrand, G., Decourchelle, A., Ballet, J., Teyssier, R., & Fraschetti, F. 2010, A&A, 509, L10
Frail, D. A., Goss, W. M., Reynoso, E. M., et al. 1996, AJ, 111, 1651
Freeman, P., Doe, S., & Siemiginowska, A. 2001, Proc. SPIE, 4477, 76
Ghavamian, P., Laming, J. M., & Rakowski, C. E. 2007, ApJL, 654, L69
Giordano, F., Naumann-Godo, M., Ballet, J., et al. 2012, ApJL, 744, L2
Giuliani, A., Cardillo, M., Tavani, M., et al. 2011, ApJL, 742, L30
Giuliani, A., Tavani, M., Bulgarelli, A., et al. 2010, A&A, 516, L11
Gok, F., & Sever, A. 2012, MNRAS, 423, 1215
Hewitt, J. W., Rho, J., Andersen, M., et al. 2009, ApJ, 694, 1266
Kamae, T., Karlsson, N., Mizuno, T., et al. 2006, ApJ, 647, 692
Kim, Y., Rieke, G. H., Krause, O., et al. 2008, ApJ, 678, 287
Koo, B.-C., Heiles, C., Stanimirović, S., et al. 2010, AJ, 140, 262
Koo, B.-C., Kim, K.-T., & Seward, F. D. 1995, ApJ, 447, 211
Lee, H.-G. 2005, JKAS, 38, 385
Lee, H.-G., Moon, D.-S., Koo, B.-C., et al. 2011, ApJ, 740, 31
Lozinskaya, T. A. (ed.) 1992, Supernovae and Stellar Wind in the Interstellar Medium (Melville, NY: AIP)
Mattox, J. R., Bertsch, D. L., Chiang, J., et al. 1996, ApJ, 461, 396
McClure-Griffiths, N. M., Dickey, J. M., Gaensler, B. M., et al. 2005, ApJS, 158, 178
McKee, C. F., & Ostriker, J. P. 1977, ApJ, 218, 148
Milne, D. K., & Dickel, J. R. 1975, AuJPh, 28, 209
Mori, M. 2009, APh, 31, 341
Morlino, G., & Caprioli, D. 2012, A&A, 538, A81
Nolan, P. L., Abdo, A. A., Ackermann, M., et al. 2012, ApJS, 199, 31
Pei, Y. C. 1992, ApJ, 395, 130
Pinheiro Gonçalves, D., Noriega-Crespo, A., Paladini, R., et al. 2011, AJ, 142, 47
Rando, R. for the Fermi LAT Collaboration. 2009, arXiv:0907.0626
Raymond, J. C., Cox, D. P., & Smith, B. W. 1976, ApJ, 204, 290
Raymond, J. C., & Smith, B. W. 1977, ApJS, 35, 419
Reach, W. T., Rho, J., & Jarrett, T. H. 2005, ApJ, 618, 297
Reach, W. T., Rho, J., Tappe, A., et al. 2006, AJ, 131, 1479
Reynolds, S. P. 2008, ARA&A, 46, 89
Reynolds, S. P., & Keohane, J. W. 1999, ApJ, 525, 368
Rho, J., & Petre, R. 1998, ApJL, 503, L167
Salpeter, E. E. 1977, ARA&A, 15, 267
Sault, R. J., Teuben, P. J., & Wright, M. C. H. 1995, in ASP Conf. Ser. 77, Astronomical Data Analysis Software and Systems IV, ed. R. A. Shaw, H. E. Payne, & J. J. E. Hayes (San Francisco, CA: ASP), 433
Shaver, P. A., & Goss, W. M. 1970, AuJPA, 14, 133
Slane, P., Smith, R. K., Hughes, J. P., et al. 2002, ApJ, 564, 284
Smith, R. K., & Hughes, J. P. 2010, ApJ, 718, 583
Strong, A. W., Moskalenko, I. V., & Reimer, O. 2000, ApJ, 537, 763
Tang, Y. Y., Fang, J., & Zhang, L. 2011, ApJ, 739, 11
Tavani, M., Giuliani, A., Chen, A. W., et al. 2010, ApJL, 710, L151
Troja, E., Bocchino, F., Miceli, M., & Reale, F. 2008, A&A, 485, 777
Truelove, J. K., & McKee, C. F. 1999, ApJS, 120, 299
Uchiyama, Y., Blandford, R. D., Funk, S., et al. 2010, ApJL, 723, L122
Uchiyama, Y., Funk, S., Katagiri, H., et al. 2012, ApJL, 749, L35
Wardle, M., & McDonnell, K. 2012, in IAU Symp. 287, Cosmic Masers—From OH to H0, ed. R. S. Booth, W. H. T. Vlemmings, & E. M. L. Humphreys (Cambridge: Cambridge Univ. Press), 441
White, R. L., & Long, K. S. 1991, ApJ, 373, 543
Whiteoak, J. B. Z., & Green, A. J. 1996, A&AS, 118, 329
Williams, J. P., Blitz, L., & Stark, A. A. 1995, ApJ, 451, 252
Wu, J. H. K., Wu, E. M. H., Hui, C. Y., et al. 2011, ApJL, 740, L12
Yoshida, K. 2008, AdSpR, 42, 477
Yusef-Zadeh, F., Wardle, M., Rho, J., et al. 2003, ApJ, 585, 319
Zhang, W., MacFadyen, A., & Wang, P. 2009, ApJL, 692, L40